Temporal analysis of acoustic emission from a plunged granular bed

Daisuke Tsuji and Hiroaki Katsuragi*
Department of Earth and Environmental Sciences, Nagoya University, Furocho, Chikusa, Nagoya 464-8601, Japan
(Received 27 April 2015; published 13 October 2015)

The statistical property of acoustic emission (AE) events from a plunged granular bed is analyzed by means of actual-time and natural-time analyses. These temporal analysis methods allow us to investigate the details of AE events that follow a power-law distribution. In the actual-time analysis, the calm-time distribution, and the decay of the event-occurrence density after the largest event (i.e., the Omori-Utsu law) are measured. Although the former always shows a power-law form, the latter does not always obey a power law. Markovianity of the event-occurrence process is also verified using a scaling law by assuming that both of them exhibit power laws. We find that the effective shear strain rate is a key parameter to classify the emergence rate of power-law nature and Markovianity in granular AE events. For the natural-time analysis, the existence of self-organized critical states is revealed by calculating the variance of natural time χ_k, where kth natural time of N events is defined as $\chi_k = k/N$. In addition, the energy difference distribution can be fitted by a q-Gaussian form, which is also consistent with the criticality of the system.

DOI: 10.1103/PhysRevE.92.042201 PACS number(s): 83.80.Fg, 45.70.−n, 46.40.−f, 81.05.Rm

I. INTRODUCTION

Power-law distributions can be observed in various fields of natural and artificial phenomena [1]. Examples include the distribution of incomes (Pareto's law), the frequency of appearance of English words (Zipf's law), the number of meteorites impacting on a planet, and the number of species per genus in flowering plants [2]. For seismic activity, one of the best-known power-law relations is the Gutenberg-Richter (GR) law [3]:

$$G(Q) \sim Q^{-\gamma}, \tag{1}$$

where Q, $G(Q)$, and γ are the emitted energy per event, its frequency of occurrence, and a characteristic exponent (positive constant), respectively. Recently, experiments and simulations of soft materials which are related to seismic activity have been performed. These studies have reported various power-law event-size distributions (e.g., sliding friction of gels [4] and granular avalanches in simulations [5]). Although this kind of power-law event-size distribution has also been discovered in many natural phenomena (e.g., forest fire areas [6], floods [7], fragments [8], and Tsunami runup heights [9]), they are empirical laws and not fully understood in terms of their physical origin.

The physical mechanisms determining the power-law exponent have long been studied. For instance, the exponent of the power-law size distribution in brittle fragmentation shows particular relations to the higher order moment and system size [10–12]. Besides, the exponent value depends on the dimensionality and the manner of crack propagation [8]. Also, stress relaxation mechanisms in plastic deformation can be classified by the power-law exponent of stress drop distributions [13]. Although some fundamental aspects concerning the power-law size distributions have been revealed as mentioned, much deeper investigation associated with the appropriate classification of the system is necessary for truly understanding the universality of the whole power-law distributions.

In this study, acoustic emission (AE) burst events emitted from a plunged granular bed are particularly examined. In Ref. [14], the behavior of granular matter has been studied using AE technique, in which the size distribution of AE burst events obeys a power law. In the experiment, the power-law exponent [γ in Eq. (1)] varies depending on the experimental conditions. Although the exponent value was related to the mode of deformation (brittle-like or plastic-like), the analysis was still very qualitative in Ref. [14]. Thus, further detailed analyses are necessary to identify the underlying physical mechanisms governing the power-law nature of granular AE events. Such a deeper understanding of granular AE events might also provide a universal framework for various power-law distributions. Moreover, because the statistical behavior of dry granular matter is somewhat similar to that of seismicity [15], the detailed study of granular behavior could be helpful to understand geophysical phenomena as well.

The most serious deficiency in previous analyses of AE event-size distributions is the lack of temporal information. A power-law event-size distribution such as the GR law usually neglects the time series of event occurrence. It only deals with the size of events, while the events indeed occur in time series. In order to consider the temporal information, here we employ two analysis methods: actual-time and natural-time analyses.

In the actual-time analysis, the amplitude of events is omitted, in contrast to the analysis of event-size distributions such as the GR law. Then the time interval between successive AE events, called *calm time* (a.k.a. interoccurrence time or waiting time), and the event-occurrence density are measured. The distribution of calm time has been found to be power law in many AE measurements (e.g., tensile failure experiment on paper sheets [16] and volcanic rocks at Stromboli [17]). For the event-occurrence density, the power-law decay of aftershock activity is known as the Omori-Utsu (OU) law in seismology [18,19]. OU-like behavior is also observed in various AE measurements (e.g., microfracturing in a compressed rock [20,21]).

If both these quantities (calm time and event-occurrence density) exhibit power-law distributions and each power-law exponent can be determined, we can evaluate Markovianity

*katsurag@eps.nagoya-u.ac.jp

of the event time series using these exponents. This powerful method to verify Markovianity was first developed for analyzing real seismic data, and the non-Markov nature of real seismic activity was revealed by Abe and Suzuki [22,23]. In the current study, we discuss the statistical properties of granular AE events by applying this method to the granular AE event data.

Natural-time analysis, on the other hand, discards calm-time information. It only uses the order of events and corresponding amplitudes. The idea of natural time has also been proposed for the analysis of seismicity [24–34]. For an event time series comprising N events, natural time χ_k serves as an index for the occurrence of the kth event and is defined as $\chi_k = k/N$. Then the variance κ_1 is computed as

$$\kappa_1 = \sum_{k=1}^{N} p_k \chi_k^2 - \left(\sum_{k=1}^{N} p_k \chi_k \right)^2 = \langle \chi^2 \rangle - \langle \chi \rangle^2, \qquad (2)$$

where $p_k = Q_k / \sum_{i=1}^{N} Q_i$ is the normalized released energy Q_k in the kth event. Seismic electrical signals right before earthquakes tend to show a critical value $\kappa_1 = 0.07$ [24]. Similar κ_1 behaviors can be confirmed in some self-organized critical systems [31–34], the original concept of which was introduced by Bak *et al.* [35]. Furthermore, AE signals from the deformed rock have exhibited behavior similar to seismicity in terms of the natural-time analysis [36].

In this study, the temporal properties of AE events emitted from a plunged granular bed are thoroughly investigated through these analyses. The relation between the measured results and the previously obtained event-size distributions (GR law) [14] is also discussed on the basis of the experimental data.

II. EXPERIMENT

The experimental methodology and data used in this study are the same as those in Ref. [14]. Glass beads (grain diameter $d = 0.4, 0.8,$ or 2.0 mm) are poured into a cylindrical Plexiglas container. A steel sphere (radius $r = 5$, 10, or 20 mm) is then penetrated into the granular bed. The penetration speed is fixed as $v = 0.5$, 1.0, or 5.0 mm s^{-1}. The top surface of the granular bed is open to the atmosphere and any confining pressure is not applied to the bed. An AE sensor (NF AE-900s-WB) is buried and fixed in the granular bed to capture AE events created by the penetration. The AE sensor is a piezoelectric transducer which converts dynamic motions (e.g., ultrasonic elastic wave) into electric signals [37]. Because the AE signals are very weak, they are amplified by an amplifier (NF AE-9913) and a discriminator (NF AE-9922). The sampling rate of the AE data is 1 MHz. Three experimental realizations for each set of experimental conditions are performed to check the reproducibility. In general, granular behaviors have a strong memory effect and history dependence [38]. The sphere penetration must leave its memory in the granular bed such as the force chain structure in a tapped granular bed [39]. Thus, a fresh granular bed is deposited before every experimental run to erase the memory of penetration.

Let us summarize the experimental results briefly. A raw data example of AE signals A (in V) as a function of time is shown in Fig. 1(a). While the origin of time in Fig. 1(a) is

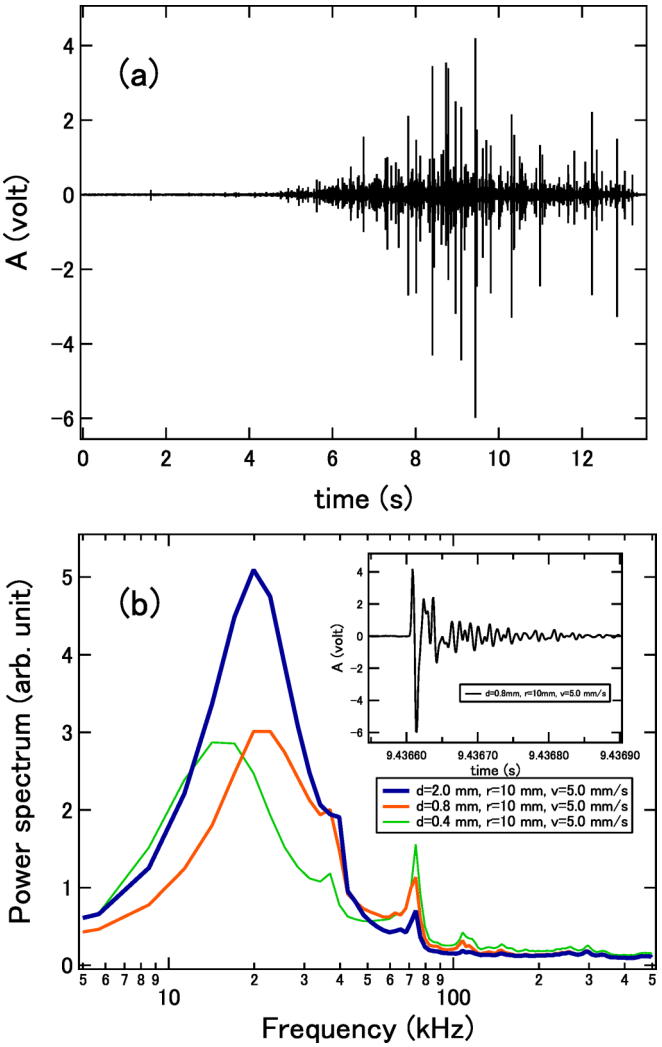

FIG. 1. (Color online) (a) Example of AE signals during the penetration of a sphere into a glass-bead bed. (b) Average power spectra of AE events produced per penetration for some experimental conditions. Inset: An example of typical attenuating oscillation with a short decay time.

defined by $z = 0$ (z is the penetration depth of the intruder), similarly to Ref. [14], it is arbitrary in the current study. Actually, the origin of time $t = 0$ is defined later by the main event. The corresponding experimental conditions are $d = 0.8$ mm, $r = 10$ mm, and $v = 5.0$ mm s^{-1}. Henceforth, we use these experimental conditions for subsequent plots shown in this paper unless otherwise noted. Because all AE events show typical attenuating oscillation with a short decay time as depicted in the inset in Fig. 1(b), each AE event can be picked up from the measured AE signals using a threshold value $A_{\rm th} = 0.06$ V and deadtime $t_{\rm dead} = 300$ μs [14]. The total number of AE events identified by this method ranges from 10^2 to 10^4. Figure 1(b) shows average power spectra of AE events for several experimental conditions. The dominant frequencies, 20 and 75 kHz, seem to be independent of the experimental conditions and might result from complex coupling of both the AE device and the granular media. For more details of the experimental setting, see Ref. [14].

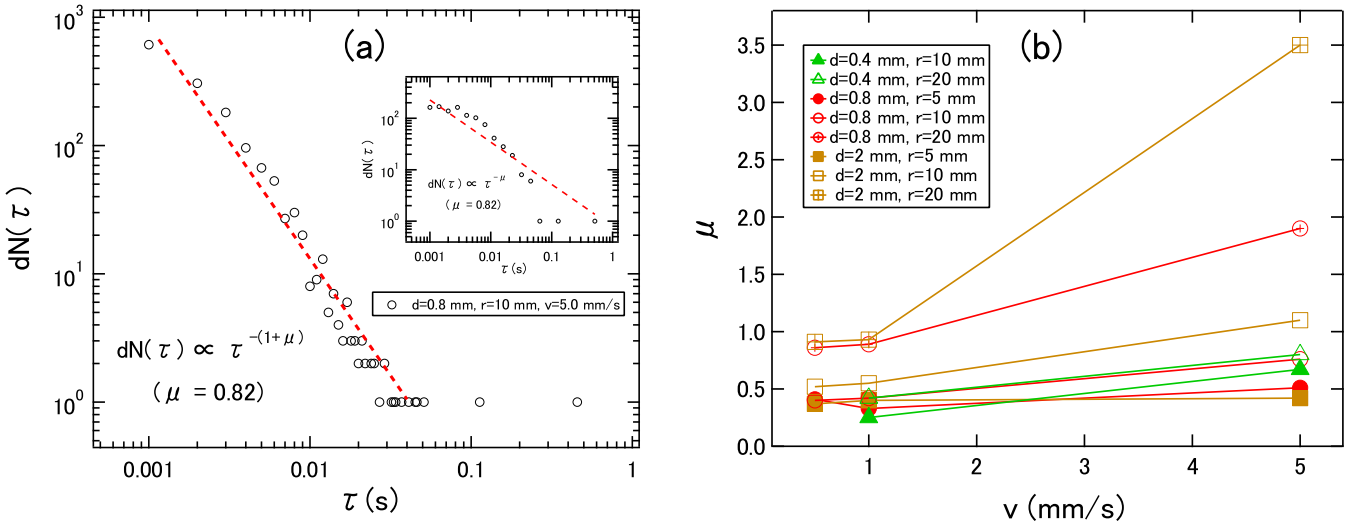

FIG. 2. (Color online) (a) Calm-time distribution $dN(\tau)$ obeying a power law [Eq. (3)]. Inset: $dN(\tau)$ with logarithmically increasing bins, where the slope corresponds to $-\mu$, not $-(1+\mu)$. Bin widths are given as $0.001(\sqrt{2})^n$ s (e.g., 0.001 s, $0.001\sqrt{2}$ s, 0.002 s,...). Dashed (red) lines in both plots show the power law with $\mu = 0.82$ obtained by the MLE method. (b) The exponent of the calm-time distribution μ as a function of the penetration speed v. The μ value depends on various experimental conditions, in contrast to γ in Eq. (1). The calm-time data used here were obtained after the main event defined in Sec. III B.

III. ACTUAL-TIME ANALYSIS

A. Calm-time distribution

First, we focus on analysis of the calm time τ, which corresponds to the time interval between two successive events. Specifically, the frequency distribution of calm time $P(\tau)$ is measured. The occurrence time of each event is determined by the moment at which the signal amplitude exceeds the threshold value $A_{\rm th}$. In Fig. 2(a), an example of a $P(\tau)$ distribution obeying the power-law form is presented. All other $P(\tau)$ distributions also exhibit power-law forms. Namely, $P(\tau)$ always obeys

$$P(\tau) = \frac{dN(\tau)}{N_{\rm tot}} \sim \tau^{-(\mu+1)}, \tag{3}$$

where $dN(\tau)$ and $N_{\rm tot}$ are the number of events with calm-time τ intervals and the total number of events in the time series, respectively. The minimum (binning) time scale used in $dN(\tau)$ measurement is 1 ms. Since the number of events is limited and the finite-size effect must be considered carefully, here we employ the method of maximum likelihood estimation (MLE) [1,40,41] to determine the exponent value. MLE determines the exponent to maximize the likelihood function L defined as

$$L(1+\mu|\tau) = \prod_{k=1}^{N} \frac{\tau_k^{-(1+\mu)}}{\zeta(1+\mu)}, \tag{4}$$

where τ_k is the calm time of the kth event normalized to the minimum value and $\zeta(1+\mu)$ is the Riemann zeta function expressed as $\sum_{k=1}^{N} k^{-(1+\mu)}$. To apply MLE, the exponent μ must be greater than 0. Otherwise, the Riemann zeta function diverges. Because MLE enables us to avoid large bias error in many frequency distributions (e.g., [40], [42], [43]), MLE is a preferred method for accurately estimating the power-law exponent. The determined μ value in the data in Fig. 2(a) is 0.82. To check the validity of the determined exponent from another aspect, the frequency distribution of τ with logarithmic bins using a constant rate $\sqrt{2}$ is shown in the inset in Fig. 2(a). Although the data in the inset are scattered, the global trend can be reproduced by the power-law fitting determined by MLE ($\mu = 0.82$).

For the obtained power-law exponent, μ depends on the experimental conditions. According to the previous study [14], the exponent of event-size distributions (GR law) γ mainly depends on the grain size d. In contrast, the exponent of the calm-time distribution $P(\tau)$ is sensitive to various parameters. Figure 2(b) shows the v dependence of the exponent μ, where v and μ are positively related. This means that the faster the penetration speed is, the more the relative frequency of shorter calm time increases.

B. Event-occurrence density distribution

Second, the number of events occurring per unit time after the main event $S(t)$ is considered. $S(t)$ is defined by

$$S(t) = \frac{dN'(t)}{dt} \sim t^{-p}, \tag{5}$$

where p is a characteristic exponent, t stands for the time elapsed after the main event, and $dN'(t)$ is the number of events occurring in the short time interval between t and $t+dt$. We call $P(t)$ the *event-occurrence density*. Because the time $t = 0$ should be defined by the moment of main-event occurrence, it is necessary to locate the main event. In usual seismic activity, the main event (main shock) can be located by subsequent smaller aftershocks [44]. Thus, in this work, we employ the largest AE event in the time series as the main event. Then the event-occurrence density after the main event is measured from the experimental data. For real seismic activity, the universal power law is well known as the OU law, which states that $S(t)$ decays with time following a power-law relationship expressed

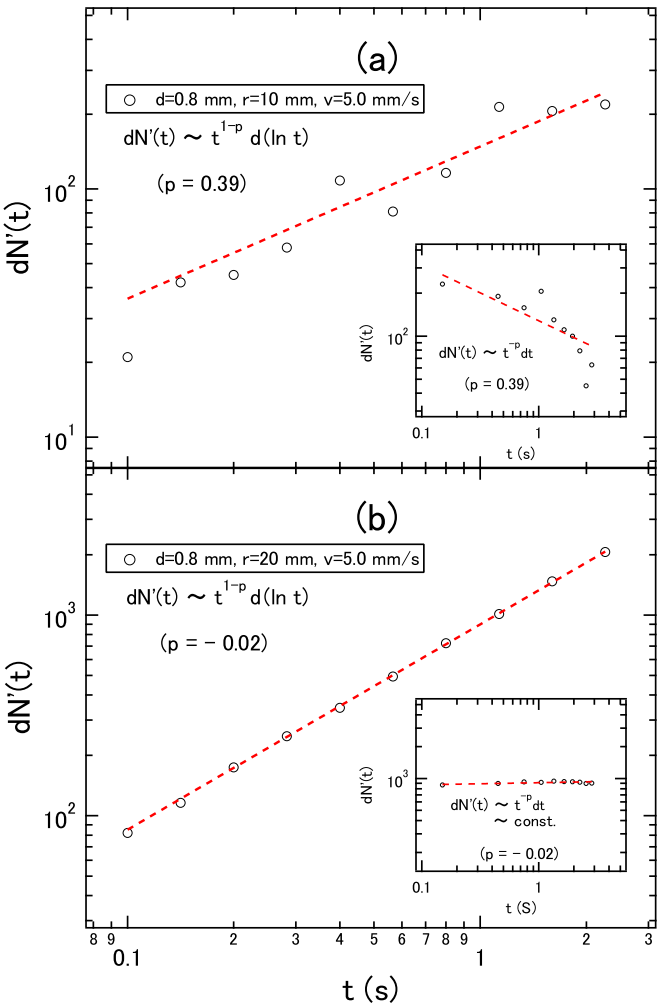

FIG. 3. (Color online) Power-law histograms with logarithmic bins of the event-occurrence density decay for (a) a nonsteady (OU-like) AE event and (b) a steady (constant) AE event. Since the main plots show the logarithmically binned data, OU law is expressed as $dN'(t) = t^{1-p} d\ln t$. Here, the range $dt = 0.1(\sqrt{2})^0 - 0.1(\sqrt{2})^9$ s is used. The least-squares method is used to determine the p value. Insets: Power-law histograms $dN'(t) \sim S(t)dt$ with the constant linear binning $dt = 0.3$ s.

on the right-hand side in Eq. (5). The exponent p usually ranges from 0.8 to 1.5 for real seismic activity [30].

However, the current experimental result shows various behaviors. Some $dN'(t)$ distributions follow power-law-like decay [inset in Fig. 3(a)]; others seem to be almost constant [inset in Fig. 3(b)]. The former and latter correspond to the nonsteady and steady processes, respectively. The nonsteady process means the existence of the main event followed by power-law-like decay of subsequent aftershock-like AE events. In other words, the meaningful main event cannot be identified in the latter (steady) case. Actually, even in the power-law (nonsteady) case, the scaled range is not very wide (only one order of magnitude) as shown in the inset in Fig. 3. This implies that it is not very easy to confirm a clear OU law (power-law decay of aftershocks) in granular AE events. Although the decay range is limited, the insets in Figs. 3(a) and 3(b) are significantly different. To discriminate these two phases and discuss the statistical property from the aspect of Markovianity, here we assume the power-law form for $dN'(t)$. The estimated power-law exponent values will play a crucial role to characterize the AE event statistics.

In contrast to the calm-time distributions, which show clear power-law behavior, care must be taken in precisely determining the fitted p value for event-occurrence density distributions. Because most of the fitted p values appear to be less than 1, the method of MLE cannot be used due to the divergence of the Riemann zeta function. Instead, logarithmically increasing bins are employed here. Unequal bin widths are usually used to obtain a more homogeneous number of data per bin than that with a constant bin width, which can reduce statistical errors in the power-law tail due to the poor number of samples [41,45]. Here, the bin widths are given by $0.1(\sqrt{2})^n$ s (e.g., $0.1, 0.1\sqrt{2}, 0.2, \ldots$ s). Figures 3(a) and 3(b) show histograms of the number of aftershock-like events $dN'(t)$ after the main event obtained using the logarithmic bins. By applying the logarithmic binning, the power-law exponent of the data plot varies as

$$\frac{dN'(t)}{d\ln t} \sim S(t)t \sim t^{1-p}. \tag{6}$$

Namely, the slopes in the main plots in Fig. 3 correspond to $1-p$. Although the data scatter considerably in Fig. 3(a), we assume the power-law behavior at least in the range of $0.1 < t < 3$ s. Then the Markovianity of the event series after the main event can be evaluated as discussed in Sec. III C. Using this procedure, all the data are fitted by power-law forms. The fitted p values for Figs. 3(a) and 3(b) are 0.39 and -0.02, respectively. The corresponding slopes are also shown in the insets.

In Fig. 4, the histogram of the fitted p values for the whole data set is presented. As shown in Fig. 4, the histogram shows a bimodal distribution and the valley around $p = 0.3$ seems to discriminate two phases. Thus, we define the case of $p > 0.3$ as nonsteady (OU-like) states. One can also confirm a small

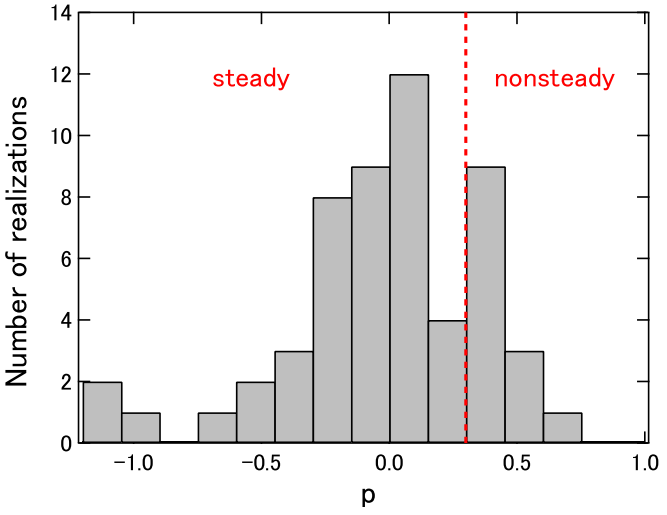

FIG. 4. (Color online) Histogram of the fitted p value showing a bimodal structure. To distinguish nonsteady (OU-like) distributions from steady distributions, the value at the valley between two peaks ($p = 0.3$) is used [dashed vertical (red) line].

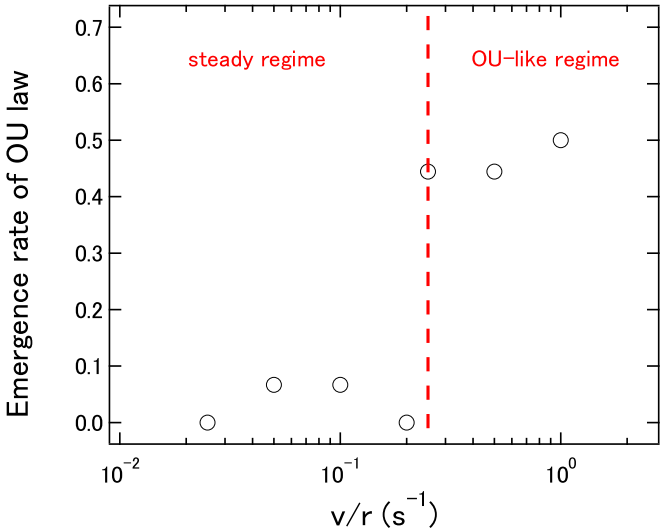

FIG. 5. (Color online) Effective shear strain rate (v/r) dependence of the emergence rate of OU-like behavior. The larger shear strain rate ($v/r \geqslant 0.25\ \mathrm{s}^{-1}$) tends to cause more OU-like behaviors than the small shear strain rate ($v/r < 0.25\ \mathrm{s}^{-1}$). We express these two distinctive regimes as *steady* and *OU-like* (nonsteady) regimes.

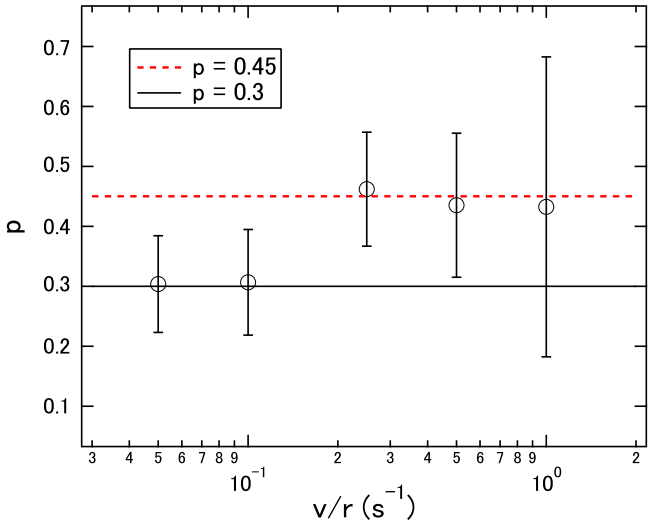

FIG. 6. (Color online) Effective shear strain rate (v/r) dependence of the fitted p value. The dashed (red) line represents the level $p = 0.45$, while the solid black line refers to the marginal value $p = 0.3$. The p value obtained in the OU-like regime ($v/r \geqslant 0.25\ \mathrm{s}^{-1}$) is almost independent of v/r.

portion of the population in the negative-p regime. This might be interesting behavior, possibly indicating the precursor of the large event. However, here we only focus on the power-law *decay* corresponding to the OU-like state.

As discussed thus far, some experiments show OU-like behavior and others do not. What is the most important parameter determining the behavior of the event-occurrence density? To answer this question, we study some parameter dependencies and find that the effective shear strain rate v/r (the penetration speed divided by the radius of a penetrator) [38] is relevant to characterize the state. Specifically, the emergence rate of OU-like states is shown as a function of v/r in Fig. 5. The emergence rate of the OU law is defined by the ratio of the experimental realizations showing $p > 0.3$ to the total experimental realizations with an identical v/r. Since the number of experimental realizations with an identical v/r is not constant, we employ the normalized occurrence ratio to estimate the emergence frequency. One can confirm that the emergence rate of the OU law (nonsteady state) abruptly increases at $v/r \geqslant 0.25\ \mathrm{s}^{-1}$. Although the complete reproducibility of OU-like behavior is not established even in the range of $v/r \geqslant 0.25\ \mathrm{s}^{-1}$, Fig. 5 implies that $v/r = 0.25\ \mathrm{s}^{-1}$ is the marginal value between the steady and the nonsteady (OU-like) regime.

Next, to verify the v/r dependence of p, the averaged p value of the OU law is plotted as a function of v/r in Fig. 6. In the OU-like regime ($v/r \geqslant 0.25\ \mathrm{s}^{-1}$), the p values show a roughly constant value, $p \simeq 0.45$, in contrast to the steady regime, suggesting $p \simeq 0.3$, which might result from the defined marginal value between the steady regime and the OU-like regime ($p = 0.3$). Since the emergence rate of OU-like behavior is very low at $v/r < 0.25\ \mathrm{s}^{-1}$, the value is sensitive to the threshold. However, the data errors in Fig. 6 are considerably large, thus the difference between $p = 0.3$ and $p = 0.45$ is not very clear.

C. Markov scaling

Using two exponents, μ and p, defined in Eqs. (3) and (5), the Markovianity of the event time series after the main event can be discussed in terms of a scaling law. The specific values used in the evaluation of the Markov scaling are μ (Fig. 2) and p (Fig. 6) computed from the data after the main event. The scaling law used here was originally developed and applied to real seismicity. As a result, a non-Markov nature of earthquake aftershocks was reported [22,23]. Here, we slightly expand this scaling law. If a process of event occurrence is Markovian, the following equation holds [46]:

$$S(t) = P(t) + \int_0^t P(t-t')S(t')dt', \tag{7}$$

which can be derived from the Kolmogorov forward equation [47]. Then the Laplace transformation of Eq. (7) yields

$$\mathcal{L}[S](s) = \frac{\mathcal{L}[P](s)}{1 - \mathcal{L}[P](s)}, \tag{8}$$

where $\mathcal{L}[f](s) = \int_0^\infty e^{-st} f(t)dt$. Here, we assume that both $P(t)$ and $S(t)$ decay following the power-law forms as written in Eqs. (3) and (5) for a large value of t. Then the Laplace transformations of $P(t)$ and $S(t)$ result in different expressions depending on the ranges of the exponents. If the exponents μ and p are in the ranges

$$0 < \mu < 1 \quad \text{and} \quad 0 < p < 1, \tag{9}$$

the Laplace transformations of $P(t)$ and $S(t)$ behave as

$$\mathcal{L}[P](s) \sim 1 - \alpha s^{\mu}, \tag{10}$$

$$\mathcal{L}[S](s) \sim \frac{1}{s^{1-p}} \tag{11}$$

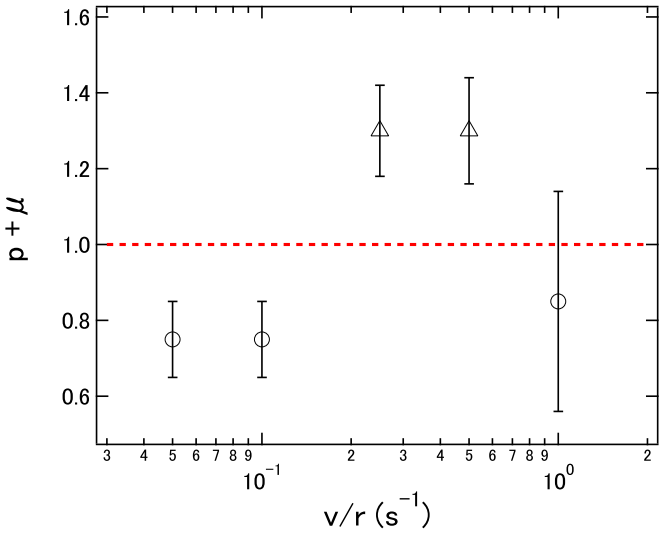

FIG. 7. (Color online) $p+\mu$ as a function of the effective shear strain rate v/r. The dashed horizontal (red) line indicates the level $p+\mu=1$ (Markov scaling law). Circles are distributed around $p+\mu\simeq 1$ (or $p+\mu\lesssim 1$); triangles, clearly above this value.

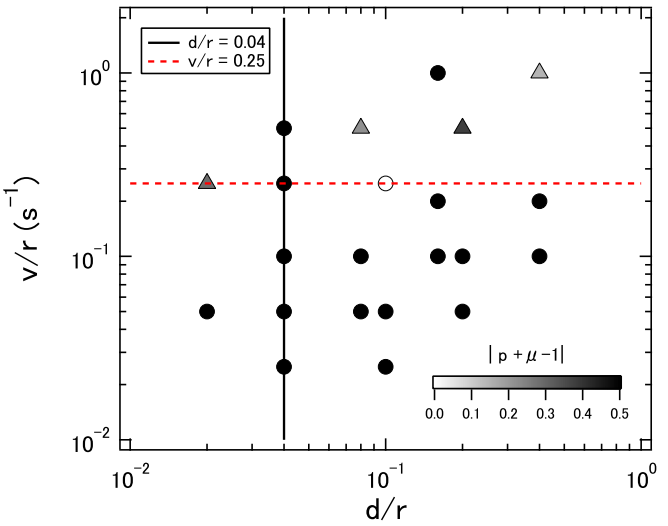

FIG. 8. (Color online) Phase diagram of the temporal statistics of granular AE events. The x and y axes represent d/r and v/r, respectively. The meaning of each symbol is as follows. Triangles represent cases in which nonsteady (OU-like) behaviors are observed. Note that a triangle does not indicate the complete reproducibility of OU-like behavior. As mentioned in the text, three experimental realizations of each experimental condition were carried out. When two of three realizations showed OU-like behavior, a triangle is used. The gray scale in triangles indicates the value of $|p+\mu-1|$ as shown in the legend. The open circle indicates the steady Markov process ($1<\mu<2$, $p\simeq 0$), while filled circles indicate the steady non-Markov process ($0<\mu<1$ or $2<\mu$, $p\simeq 0$). The vertical line $d/r=0.04$ is the boundary between the brittle-like and the plastic-like regimes [14]. The dashed horizontal (red) line at $v/r=0.25$ s^{-1} is considered to be the characteristic shear strain rate above which OU-like behavior can often be observed.

for a small limit of s, where α is a positive constant. Substituting Eqs. (10) and (11) into Eq. (8), we obtain a simple scaling relation [22,23]:

$$p+\mu=1. \tag{12}$$

However, if the exponent μ lies in the range

$$1<\mu<2, \tag{13}$$

the resultant Laplace transformation becomes

$$\mathcal{L}[P](s)\sim 1-\beta s \tag{14}$$

for a small limit of s, where β is a positive constant. Using Eqs. (11) and (14), Eq. (8) results in

$$p=0. \tag{15}$$

Note that this result is inconsistent with the assumed range of Eq. (9); this implies that Eq. (15) is only an asymptotic solution. In the case of $\mu>2$, the scaling relation fulfilled in a Markov process does not exist.

Equation (12) indicates the criterion for Markovianity in an OU-like (nonsteady) event time series in the range of Eq. (9). To verify Markovianity of the granular aftershock-like AE events showing OU-like behavior, $p+\mu$ as a function of v/r is depicted in Fig. 7. The dashed (red) line in Fig. 7 indicates the Markov scaling law [Eq. (12)]. One can confirm that some data (triangles) show clearly large values ($p+\mu>1$) that are somewhat similar to those of earthquake aftershocks [22,23]. In the current experimental result, however, the other data points (circles) are distributed around $p+\mu\simeq 1$ (or $p+\mu\lesssim 1$). This means that there might be a certain parameter range in which the event time series can be regarded as a Markov process. This result is contrary to real seismic activity, which always shows $p+\mu>1$, i.e., a non-Markov property.

Actually, the effective shear strain rate v/r is not a unique parameter to characterize the system. To describe the global behavior of all granular AE events in this study, the normalized grain size d/r is also used here. Indeed, d/r can be a characteristic parameter to classify the event-size distribution (GR law) [14]. $d/r=0.04$ is regarded as a marginal value between brittle-like and plastic-like behavior. As discussed in the last subsection, on the other hand, $v/r=0.25$ s^{-1} is considered a marginal value between the steady and the nonsteady (OU-like) states. Therefore, we show a phase diagram in Fig. 8, where the vertical and horizontal axes indicate the effective shear strain rate v/r and normalized grain size d/r, respectively. Although it is difficult to draw clear phase boundaries, there might be several classes of behavior in the phase diagram. In the large-v/r and large-d/r regime, the nonsteady (OU-like) event time series, which is shown by triangles, can be frequently observed. In this OU-like regime, the value of $|p+\mu-1|$ is indicated by the gray scale in each triangle as long as μ is less than 1 [i.e., the range defined by Eq. (9)]. Namely, the dark triangle means that the process is non-Markov. The steady ($p\simeq 0$) cases are represented by circles. Open and filled circles correspond to steady Markov ($1<\mu<2$, $p\simeq 0$) and steady non-Markov ($0<\mu<1$ or $2<\mu$, $p\simeq 0$), respectively.

IV. NATURAL-TIME ANALYSIS

A. Variance κ_1

Next, the natural-time analysis is applied to the identical data set. In the definition of natural time, calm time is completely neglected. Instead, the order and magnitude of events are utilized to characterize the event statistics. By simply applying Eq. (2) to the data set, we can readily calculate κ_1. Here we use the squared maximum amplitude of each AE event for its released energy value Q_k [14]. Some examples of $\kappa_1(k)$ are shown in Fig. 9. As expected, κ_1 appears to fluctuate around $\kappa_1 \simeq 0.07$ in some data, which indicates the criticality of the system. However, this tendency is not universal. For instance, the asymptotic value of $\kappa_1(k)$ in Fig. 9(c) appears to be different from 0.07. To verify the κ_1 behavior in more detail, the probability density function (PDF) of κ_1 is computed by the following procedure [28,30]. First, the κ_1 value is computed from the natural-time windows for 6–40 consecutive events. Second, this process is performed for all events by scanning the whole data set. Figure 10 shows the PDF computed from the data used in Fig. 9. The most probable value $\kappa_{1,p}$ estimated by the peak location of the PDF depends on the experimental conditions. Particularly, the grain diameter d seems to be an important parameter. This d-dependent tendency is similar to the behavior of γ in Eq. (1) (event-size distribution exponent) [14].

B. Returns distribution

Although the measurement of κ_1 is easy and useful to briefly characterize the critical state in the time series, it is in general not sufficient to evaluate the criticality of the event time series. Caruso *et al.* [48] have suggested another way to characterize the criticality in the system.

The variable *returns* $x(k)$ are defined as $x(k) = Q_{k+1} - Q_k$. Namely, $x(k)$ corresponds to the energy difference between two successive events. Here the returns are normalized to the mean $\langle x \rangle$ and standard deviation σ, $\xi = (x - \langle x \rangle)/\sigma$. Then the PDF of ξ is calculated for each experimental condition (e.g., inset in Fig. 11). As a result, it is clarified that the functional form of the PDF is independent of the experimental conditions. Therefore, to obtain better statistics, all the data on the normalized returns under various experimental conditions are merged into a single PDF. The entire PDF as a function of ξ is shown in the main plot in Fig. 11, in which the PDF has much broader tails than a normal Gaussian distribution, $f(\xi) = \exp(-\xi^2/2)/\sqrt{2\pi}$ (dashed black curve). Instead, the q-Gaussian form $f(\xi) = A_q[1 - (1-q)\xi^2/B_q]^{1/(1-q)}$ fits the data well [solid (red) curve], where A_q and B_q are

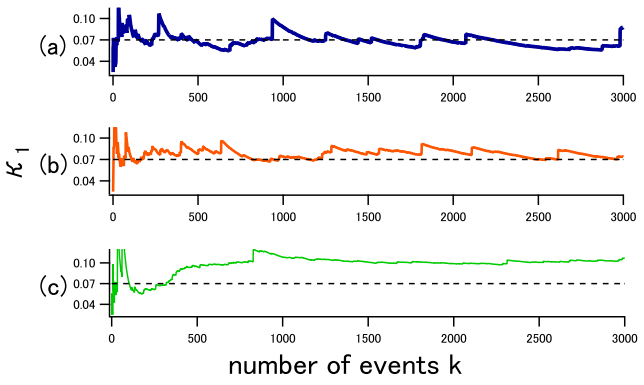

FIG. 9. (Color online) Evolution of κ_1 as a function of the number of events k for various experimental conditions: (a) $d = 2.0$ mm, (b) $d = 0.8$ mm, and (c) $d = 0.4$ mm. Other parameters are fixed at $r = 10$ mm and $v = 5.0$ mm s^{-1}. The evolutions of each κ_1 are shown up to $k = 3000$. Dashed horizontal black lines represent $\kappa_1 = 0.07$, indicating the criticality of the system. (a, b) Data fluctuate around 0.07; (c) data are clearly offset.

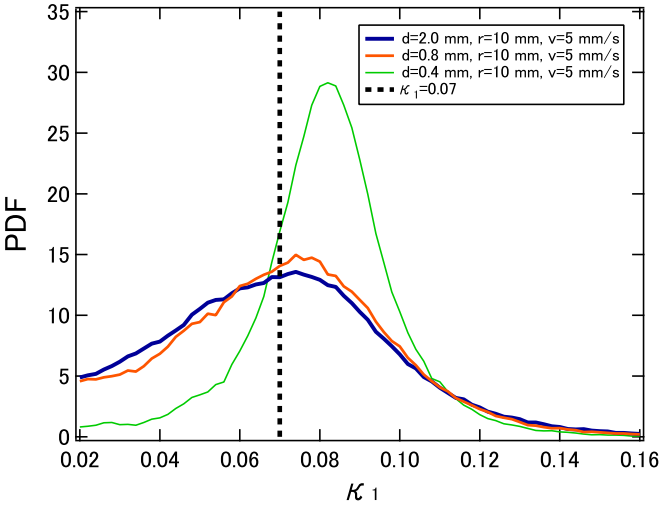

FIG. 10. (Color online) PDF of the κ_1 value under the same experimental conditions as in Fig. 9. The color code is identical to that in Fig. 9. The dashed vertical line indicates $\kappa_1 = 0.07$. Peak values of the blue ($d = 2.0$ mm) and red ($d = 0.8$ mm) curves are around 0.07.

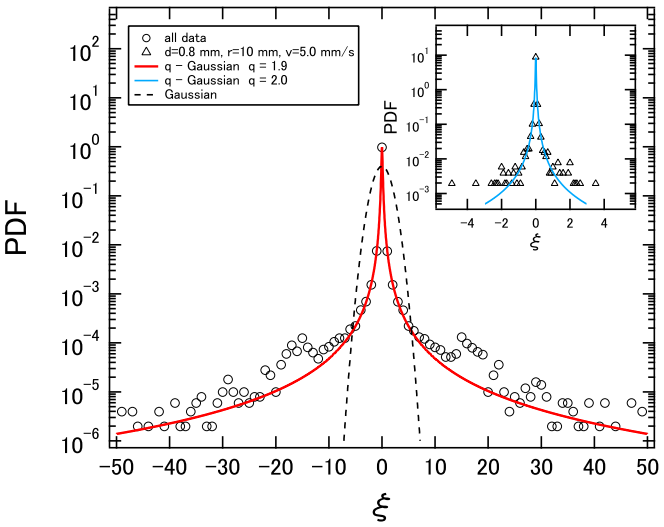

FIG. 11. (Color online) PDF of the normalized returns ξ computed from the whole AE events under all experimental conditions. Data obtained in the current experiment are better fitted by the q-Gaussian [solid (red) curve] than the normal Gaussian (dashed black curve). Inset: An example of a single PDF under the experimental conditions $d = 0.8$ mm, $r = 10$ mm, and $v = 5.0$ mm s^{-1}.

constants [49]. The computed q value is $q = 1.9$. If the data of a single experimental run are used for the PDF as shown in the inset in Fig. 11, the agreement between the q-Gaussian and the data is limited, particularly in the tail part. However, the qualitative tendency of the distribution is basically identical. Because the q-Gaussian PDF of ξ can be observed in the self-organized critical model satisfying both the power-law event-size distribution and the finite-size scaling [48], this result provides supportive evidence for the presence of the critical state.

C. Relation between κ_1 and γ

Finally, we consider the relation between natural-time analyses and event-size distributions. As shown in Figs. 9 and 10, the κ_1 value is mainly affected by the grain diameter d. Additionally, the exponent of power-law event-size distributions γ [Eq. (1)] also depends on d [14]. Thus, κ_1 and γ might show a certain relation. To check the relationship, κ_1 vs γ is plotted in Fig. 12. As expected, a correlation between them can be confirmed. The symbols (and colors) in Fig. 12 indicate the different deformation modes: the brittle-like mode, characterized by a smaller γ [(blue) circles]; and the plastic-like mode, characterized by a larger γ [(red) triangles]. The solid black curve in Fig. 12 represents a fitting by the exponentially asymptotic function $\kappa_{1,p} = 0.083 - 3.4e^{-3.1\gamma}$. The asymptotic value coincidentally agrees with $\kappa_u = 0.083$ ($\simeq 1/12$) of a *uniform* distribution [25–27,29]. In Fig. 12, $\kappa_1 = 0.07$ seems to be satisfied under the experimental conditions of brittle-like behavior. Put simply, the brittle-like regime shows $\kappa_1 \simeq 0.07$, while κ_1 approaches 0.083 with increasing γ, i.e., in a more plastic-like (flowing) regime. The condition that κ_1 approaches 0.083 means that the critical state is not established in the time series of AE events.

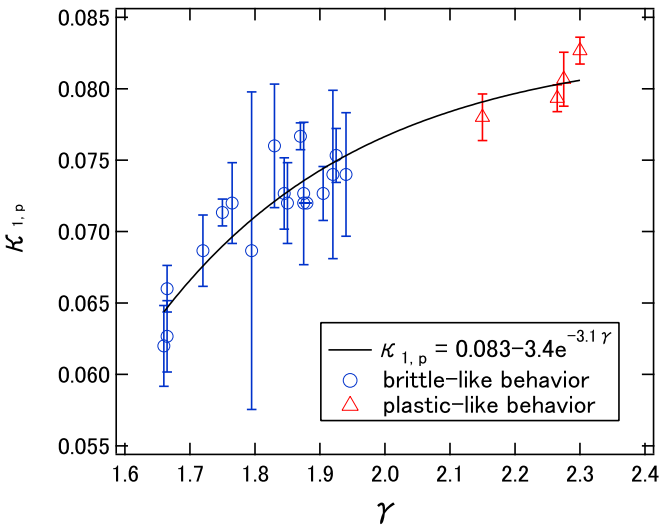

FIG. 12. (Color online) The most probable value $\kappa_{1,p}$ located by the peak of the PDF as a function of the power-law event-size distribution (GR law) exponent γ. Colors and symbols represent the difference between the brittle-like regime [(blue) circles] and the plastic-like regime [(red) triangles]. The (blue) circles tend to be distributed around 0.07. The asymptotic value estimated by the fitting is approximately 0.083, which coincidentally corresponds to κ_1 of a *uniform* distribution [25–27,29].

V. DISCUSSION

Thus far, various temporal analysis methods have been applied to the granular AE event data. Here let us discuss their physical meaning and relations.

In the actual-time analysis, power-law exponents for the calm-time distribution and the decay of the event-occurrence density were measured. All of the experimental data show power-law forms for the calm-time distribution. However, the obtained exponent value μ significantly depends on the penetration speed v. This tendency is in contrast to the case of power-law event-size distributions (GR law), in which the exponent γ is mainly determined by the grain size d and almost independent of the penetration speed v. For the event-occurrence density, power-law behavior is not universal. The emergence rate of the power-law decay (OU-like behavior) can be characterized by the effective shear strain rate v/r. Since the dimension of v/r corresponds to the inverse of time, this quantity indirectly represents a characteristic time scale in the penetration system. Additionally, the time range of OU-like behavior is equal to or less than the order of 10^0 s (e.g., Fig. 3), suggesting that the relaxation process occurs within the characteristic time scale ($0.25^{-1} = 4$ s). Therefore, it is natural that a temporal property such as the event-occurrence density can be sorted by v/r. In the range of the OU-like regime in granular AE events ($v/r \geqslant 0.25\ \mathrm{s}^{-1}$), the power-law exponent p shows an almost-constant value $p \simeq 0.45$ independent of v/r (Fig. 6). This p value is less than the typical value for real seismicity and AE events from the microfracturing of rocks, $p \simeq 1$ [21]. The reason for this discrepancy remains unsolved. Perhaps this difference originates from the peculiar nature of deformation in bulk granular matter.

For the natural-time analysis, on the other hand, the variance κ_1 is related to the exponent of the power-law event-size distribution (GR law) γ. Since the exponent γ is mainly determined by the grain size d [14], the κ_1 in granular AE event time series is also related to the grain size d. Additionally, in the natural-time analysis, the interval time between events (calm time) is completely neglected and only the order and amplitude of events are used. This is the reason why a geometrical parameter such as d or d/r becomes more essential than the temporal parameter v or v/r in the natural-time-related analysis. These two analysis methods (actual-time and natural-time analyses) are complementary to each other.

As a matter of fact, a correlation between $\kappa_{1,p}$ and γ similar to that in Fig. 12 has also been observed in artificially randomized (shuffled [27]) event series data [30]. However, the agreement remains qualitative; the specific value ranges are slightly different between the randomized event series and the current experimental data. This difference might stem from the effect of memory among events, as the randomized data do not have memory.

The statistical behavior of granular AE events becomes similar to that of real seismicity when both d/r and v/r are in the appropriate ranges: $d/r > 0.04$ and $0.25 < v/r < 1.0\ \mathrm{s}^{-1}$ (Figs. 7, 8, and 12 and Ref. [14]). In this regime, the values of γ, κ_1, and $p + \mu$ show similar values between granular AE

events and real seismic activity. Note, however, that the specific values of p and μ are different between granular AE events and real seismicity. Furthermore, this coincidence in characteristic quantities might not directly mean the correspondence of underlying physical mechanisms.

For instance, the OU law for real seismic activity can be considered as the relaxation process after the main shock. When the penetration speed is rapid, the available time for relaxation becomes relatively short (and might be insufficient) in general. Thus, it is difficult to see the relaxation in the large-v/r regime. On the other hand, a large v/r is necessary to reproduce OU-like behavior in the granular AE experiment. This implies that a large v/r might result in a large shear field, which causes a number of aftershock-like AE events. These two effects will compete with each other and the qualitative tendency seems to be the opposite. As a result, complex statistical properties are observed. To simplify the problem, a controlled experiment in a different geometrical setup should be performed. The current experimental setup actually originates from previous research concerning the slow-penetration drag force in granular matter [14,50,51]. A simpler setup such as a simple shear, which can mimic a fault slip, might be better for future studies.

VI. CONCLUSION

The statistical properties of granular AE events were investigated using two approaches: actual-time analysis (Sec. III) and natural-time analysis (Sec. IV). In the actual-time analysis, the calm-time distribution always shows a power-law form, while OU-like behavior can only be observed frequently in the range $v/r \geqslant 0.25\ \mathrm{s}^{-1}$. In the OU-like (nonsteady) regime, non-Markov behavior is observed in a particular v/r regime. However, steady (not OU-like) behavior is actually dominant in granular AE events. To control the emergence of OU-like behavior and Markovianity, the appropriate tuning of v/r (inverse of the time scale) is necessary. Natural-time analyses revealed that the κ_1 value is distributed around 0.07–0.083. In addition, q-Gaussian fits distribution of the returns (i.e., energy difference among events). This result supports the self-organized critical state of the system. The κ_1 value can be related to the exponent of power-law event-size distributions (GR law) γ. This means that the grain size d is the important parameter for κ_1 because γ is directly related to d [14]. We find that $\kappa_1 \simeq 0.07$ can be established in the brittle-like regime ($d/r > 0.04$).

In summary, statistical properties of seismic activity can be mimicked by granular AE events in the range $d/r > 0.04$ and $0.25 < v/r < 1.0\ \mathrm{s}^{-1}$. Although the current experimental system is different from the microfracturing of rocks and geological-scale phenomena, the AE data obtained from plunged granular matter exhibit some similarities to geological-scale phenomena like earthquakes in terms of actual-time and natural-time analyses.

ACKNOWLEDGMENTS

We are grateful to S. Abe, T. Hatano, S. Watanabe, H. Kumagai, S. Sirono, and T. Morota for fruitful comments and discussions. In addition, we thank K. Matsuyama for taking the data used in this study.

[1] A. Clauset, C. R. Shalizi, and M. E. J. Newman, SIAM Rev. **51**, 661 (2009).
[2] W. J. Reed, Econom. Lett. **74**, 15 (2001).
[3] B. Gutenberg and C. F. Richter, *Seismicity of the Earth and Associated Phenomena* (Princeton University Press, Princeton, NJ, 1949).
[4] T. Yamaguchi, M. Morishita, M. Doi, T. Hori, H. Sakaguchi, and J.-P. Ampuero, J. Geophys. Res.: Solid Earth **116**, B12306 (2011).
[5] T. Hatano, C. Narteau, and P. Shebalin, Sci. Rep. **5**, 12280 (2015).
[6] B. D. Malamud, G. Morein, and D. L. Turcotte, Science **281**, 1840 (1998).
[7] D. Turcotte and L. Greene, Stochas. Hydrol. Hydraul. **7**, 33 (1993).
[8] J. A. Åström, Adv. Phys. **55**, 247 (2006).
[9] S. M. Burroughs and S. F. Tebbens, Pure Appl. Geophys. **162**, 331 (2005).
[10] H. Katsuragi, D. Sugino, and H. Honjo, Phys. Rev. E **68**, 046105 (2003).
[11] H. Katsuragi, D. Sugino, and H. Honjo, Phys. Rev. E **70**, 065103 (2004).
[12] H. Katsuragi, S. Ihara, and H. Honjo, Phys. Rev. Lett. **95**, 095503 (2005).
[13] T. Niiyama and T. Shimokawa, Phys. Rev. E **91**, 022401 (2015).
[14] K. Matsuyama and H. Katsuragi, Nonlin. Process. Geophys. **21**, 1 (2014).
[15] J. Duran, *Sands, Powders, and Grains: An Introduction to the Physics of Granular Materials* (Springer, New York, 2000).
[16] L. I. Salminen, A. I. Tolvanen, and M. J. Alava, Phys. Rev. Lett. **89**, 185503 (2002).
[17] P. Diodati, F. Marchesoni, and S. Piazza, Phys. Rev. Lett. **67**, 2239 (1991).
[18] F. Omori, J. Coll. Sci. Imp. Univ. Tokyo **7**, 111 (1894).
[19] T. Utsu, Geophys. Mag. **30**, 521 (1961).
[20] T. Hirata, J. Geophys. Res.: Solid Earth **92**, 6215 (1987).
[21] I. O. Ojala, I. G. Main, and B. T. Ngwenya, Geophys. Res. Lett. **31**, L24617 (2004).
[22] S. Abe and N. Suzuki, Physica A **388**, 1917 (2009).
[23] S. Abe and N. Suzuki, Acta Geophys. **60**, 547 (2012).
[24] P. A. Varotsos, N. V. Sarlis, and E. S. Skordas, Pract. Athens Acad. **76**, 294 (2001).
[25] P. A. Varotsos, N. V. Sarlis, and E. S. Skordas, Phys. Rev. E **67**, 021109 (2003).
[26] P. A. Varotsos, N. V. Sarlis, and E. S. Skordas, Phys. Rev. E **68**, 031106 (2003).
[27] P. A. Varotsos, N. V. Sarlis, E. S. Skordas, and M. S. Lazaridou, Phys. Rev. E **70**, 011106 (2004).
[28] P. A. Varotsos, N. V. Sarlis, H. K. Tanaka, and E. S. Skordas, Phys. Rev. E **72**, 041103 (2005).

[29] P. A. Varotsos, N. V. Sarlis, E. S. Skordas, and M. S. Lazaridou, Phys. Rev. E **71**, 011110 (2005).
[30] P. A. Varotsos, N. V. Sarlis, E. S. Skordas, H. K. Tanaka, and M. S. Lazaridou, Phys. Rev. E **74**, 021123 (2006).
[31] P. A. Varotsos, N. V. Sarlis, E. S. Skordas, S. Uyeda, and M. Kamogawa, Europhys. Lett. **92**, 29002 (2010).
[32] P. A. Varotsos, N. V. Sarlis, E. S. Skordas, S. Uyeda, and M. Kamogawa, Proc. Natl. Acad. Sci. USA **108**, 11361 (2011).
[33] N. V. Sarlis, P. A. Varotsos, and E. S. Skordas, Phys. Rev. B **73**, 054504 (2006).
[34] N. V. Sarlis, E. S. Skordas, and P. A. Varotsos, Europhys. Lett. **96**, 28006 (2011).
[35] P. Bak, C. Tang, and K. Wiesenfeld, Phys. Rev. Lett. **59**, 381 (1987).
[36] F. Vallianatos, G. Michas, P. Benson, and P. Sammonds, Physica A **392**, 5172 (2013).
[37] C. U. Grosse and M. Ohtsu (eds.), *Acoustic Emission Testing* (Springer, Heidelberg, 2008).
[38] H. Katsuragi, *Physics of Soft Impact and Cratering* (Springer, Tokyo, 2016).
[39] N. Iikawa, M. M. Bandi, and H. Katsuragi, J. Phys. Soc. Jpn. **84**, 094401 (2015).
[40] M. Goldstein, S. Morris, and G. Yen, Eur. Phys. J. B **41**, 255 (2004).
[41] M. E. J. Newman, Contemp. Phys. **46**, 323 (2005).
[42] H. Bauke, Eur. Phys. J. B **58**, 167 (2007).
[43] E. P. White, B. J. Enquist, and J. L. Green, Ecology **89**, 905 (2008).
[44] T. Lay and T. C. Wallace, *Modern Global Seismology* (Academic Press, San Diego, CA, 1995).
[45] D. W. Sims, D. Righton, and J. W. Pitchford, J. Anim. Ecol. **76**, 222 (2007).
[46] F. Bardou, J. P. Bouchaud, A. Aspect, and C. Cohen-Tannoudji, *Lévy Statistics and Laser Cooling* (Cambridge University Press, Cambridge, UK, 2002).
[47] O. E. Barndorff-Nielsen, F. E. Benth, and J. L. Jensen, Adv. Appl. Prob. **32**, 779 (2000).
[48] F. Caruso, A. Pluchino, V. Latora, S. Vinciguerra, and A. Rapisarda, Phys. Rev. E **75**, 055101 (2007).
[49] C. Tsallis, M. Gell-Mann, and Y. Sato, Europhys. News **36**, 186 (2005).
[50] H. Katsuragi, Phys. Rev. E **85**, 021301 (2012).
[51] H. Katsuragi, Chem. Eng. Sci. **76**, 165 (2012).